Multifunctional Protocells for Enhanced Penetration in 3D Extracellular Tumoral Matrices

María Rocío Villegas,[†,‡] Alejandro Baeza,*[,†,‡] Achraf Noureddine,[§] Paul N. Durfee,[§,⊥] Kimberly S. Butler,[§,⊥,#] Jacob Ongudi Agola,[§,⊥] C. Jeffrey Brinker,*[,§,⊥,¶,‖] and María Vallet-Regí*[,†,‡]

[†]Departamento de Química Inorgánica y Bioinorgánica, Facultad de Farmacia, Universidad Complutense de Madrid, 28040 Madrid, Spain

[‡]Networking Research Center on Bioengineering, Biomaterials and Nanomedicine (CIBER-BBN), 28029 Madrid, Spain

[§]Center for Micro-Engineered Materials, [⊥]Chemical and Biological Engineering, and [¶]Comprehensive Cancer Center, University of New Mexico, Albuquerque, New Mexico 87131, United States

[#]Nanobiology and [‖]Advanced Materials Laboratory, Sandia National Laboratories, Albuquerque, New Mexico 87123, United States

S *Supporting Information*

ABSTRACT: The high density of the extracellular matrix in solid tumors is an important obstacle to nanocarriers for reaching deep tumor regions and has severely limited the efficacy of administrated nanotherapeutics. The use of proteolytic enzymes prior to nanoparticle administration or directly attached to the nanocarrier surface has been proposed to enhance their penetration, but the low *in vivo* stability of these macromolecules compromises their efficacy and strongly limits their application. Herein, we have designed a multifunctional nanocarrier able to transport cytotoxic drugs to deep areas of solid tumors and once there, to be engulfed by tumoral cells causing their destruction. This system is based on mesoporous silica nanocarriers encapsulated within supported lipid bilayers (SLBs). The SLB avoids premature release of the housed drug while providing high colloidal stability and an easy to functionalize surface. The tumor penetration property is provided by attachment of engineered polymeric nanocapsules that transport and controllably unveil and release the proteolytic enzymes that in turn digest the extracellular matrix, facilitating the nanocarrier diffusion through the matrix. Additionally, targeting properties were endowed by conjugating an antibody specific to the investigated tumoral cells to enhance binding, internalization, and drug delivery. This multifunctional design improves the therapeutic efficacy of the transported drug as a consequence of its more homogeneous distribution throughout the tumoral tissue.
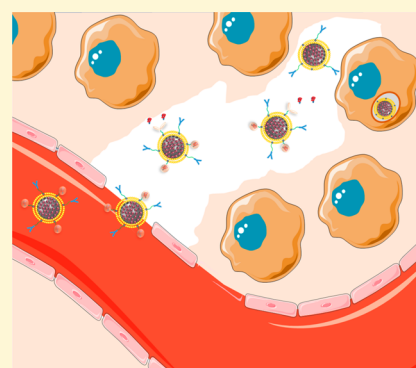
1. INTRODUCTION

Despite huge research efforts carried out in the last decades, cancer continues to be one of the leading causes of mortality worldwide.[1] Cancer cannot be considered as one simple disease. There are many different types of cancer depending on the type of malignant cell and the affected organ and even patient specific heterogeneity. Therefore, each of them presents its own set of particular features and therapeutic challenges. Moreover, even within the same tumor type, usually multiple tumor clonal cell populations coexist with different genetic alterations, which respond differently to the common administered therapeutic agents.[2] When it is not possible to remove the tumoral mass by surgery, the common treatment involves the administration of high energy radiation (radiotherapy) or the use of potent cytotoxic compounds (chemotherapy) to destroy dividing cells. However, the lack of selectivity of these therapies causes severe systemic toxicity on surrounding healthy tissues compromising not only the efficacy of the therapy, but also the patient's life or quality of life. Since Maeda and Matsumura's discovery in 1986 of passive accumulation of nanoparticles within tumoral

masses,[3] the use of nanoparticles as drug carriers has been extensively studied in oncology.[4] This phenomenon, referred to as the enhanced permeation and retention effect (EPR), is caused by the unique blood vessel architecture present in solid tumors that presents pores with diameters up to a few hundred nanometers.[5] Thus, when nanoparticles reach the tumoral area, they are extravasated into the tumor passing through these pores, whereas they cannot cross the healthy blood vessel walls. The discovery of the EPR effect triggered the development of a multitude of nanocarriers with the aim to deliver the cytotoxic compounds directly to the diseased zone, without affecting the rest of the healthy tissues.[6] These nanodevices have been engineered to possess remarkable properties such as stimuli-responsive drug release,[7] invisibility to the immune system,[8] capacity to recognize the tumoral cells,[9] or even target to the tumor stem cells.[10] However, the clinical application of

nanocarriers is still far from being a reality. A recent meta-study concluded that only 0.7% of the administered nanoparticles accumulate in the tumoral tissue, which could explain the low effectiveness of the nanotherapies observed in clinical trials.[11] One common problem in nanomedicine is the lack of system penetration into the tumoral tissue.[12] The extracellular matrix of tumoral tissues has usually a denser extracellular matrix than their healthy counterparts due to the higher presence of collagen which limits the penetration of carriers into the tissue.[13] Thus, the extravasated nanomedicine accumulates mainly on the periphery of the tumor where it can be easily flushed out of the tumor by intravasation after causing only local peripheral effects. The intratumoral administration of proteolytic enzymes such as collagenase or hyaluronidase prior to nanoparticle injection has been proposed to enhance the particle penetration.[14] These proteolytic enzymes have also been anchored on the nanocarrier surface resulting in improved particle penetration.[15] Recently, Villegas et al. reported the use of pH-responsive polymeric nanocapsules which contains collagenase for enhancing the particle penetration in 3D tumoral tissue models while protecting the proteolytic enzyme.[16] These nanocapsules were rapidly hydrolyzed under mild acidic conditions expected within hypoxic tumor tissue. In the mild acidic environment, the housed enzymes are released in 2 h, whereas nanocapsule hydrolysis requires longer times under normal physiological conditions. In addition to achieving higher penetration within the tumoral mass, an efficient nanocarrier should be able to fulfill other features such as the ability to selectively bind to the target tumoral cell within a myriad of different cell populations and retain the transported therapeutic payload until it reaches the intracellular space of the malignant cell.[17]

Herein, we report the synthesis and evaluation of a novel multifunctional nanocarrier able to penetrate deeply within a solid tumoral mass while retaining their payload and selectively bind and internalize into tumor cells where the triggered release of the cytotoxic cargo leads to destruction of the targeted tumor cell. This nanodevice is composed of a mesoporous silica nanoparticle (MSN) capable of loading high amounts of drugs due to its very high specific area and accessible interior pore volume. The MSN external surface is encapsulated within a supported lipid bilayer conjugated with proteolytic nanocapsules, targeting ligands, and polyethylene glycol (PEG) in a nanocarrier construct referred to as a protocell.[18,19]

The protocell SLB serves to protect and retain cargo within the MSN until pH triggered release within acidified endosomal environments.[19] It also confers unique properties to the system such as high colloidal stability, low immunogenicity, and long circulation times within the bloodstream. The SLB of the protocell was decorated with pH-responsive collagenase nanocapsules for enhancing tissue penetration and with EGFR-antibodies, able to selectively bind to cells that overexpress epidermal growth factor receptors (EGFR), to increase the internalization of the protocell into tumoral cells and ensuing drug delivery. The capacity of this novel multifunctional protocell to recognize EGFR-positive tumoral cells that are deeply located within a solid tumoral mass was tested employing an *in vitro* 3D cell culture model, showing significantly improved penetration, internalization and destruction capacity of the malignant cells relative to protocells prepared without collagenase nanocapsules.

2. RESULTS

2.1. Synthesis of Protocells. The protocell MSN core was designed with hexagonally arranged cylindrical pores of diameter 3−4 nm, which represents the optimal size for loading therapeutic agents based on small molecules,[20,21] as is the case for many conventional cytotoxic compounds employed in antitumoral chemotherapy.[22] MSNs were synthesized following a modified Stöber method reported elsewhere,[23] yielding monodisperse nanoparticles with an average diameter of 75−100 nm according to dynamic light scattering (DLS) measurements (Figure S1) and transmission electron microscopy (TEM) (Figure 1a). MSNs were covalently labeled with rhodamine B throughout the silica matrix to enable fluorescence imaging.
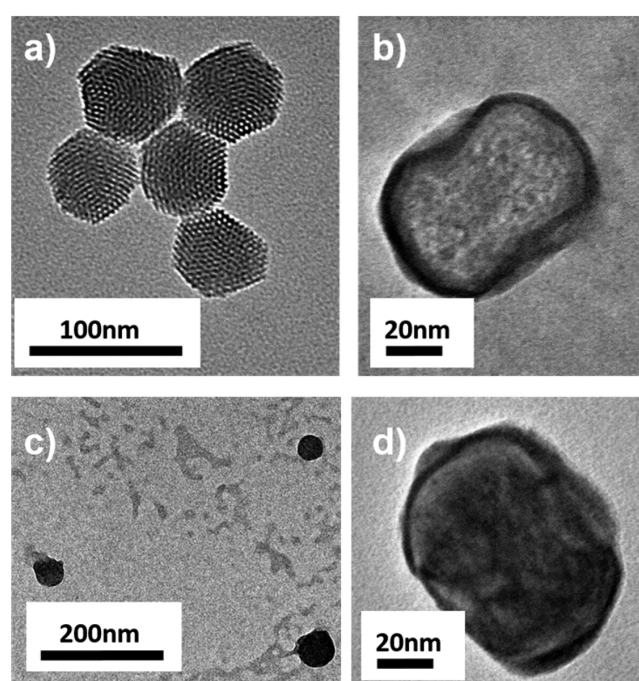

Figure 1. TEM images of (a) MSN, (b) PC−COOH13, (c) Col_{nc}, and (d) PC−COOH13-Col_{nc}.

MSNs were encapsulated within SLBs formed by fusion of zwitterionic lipid-based vesicles (Scheme 1). The zwitterionic lipid, 1,3-distearoyl-*sn*-glycero-3-phosphocholine (DSPC) was chosen as the main component to provide structural support to the liposome and cholesterol was added for controlling the fluidity of the SLB. To provide anchoring points for the further introduction of targeting moieties and collagenase nanocapsules, the functional PEGylated lipids, 1,2-distearoyl-*sn*-glycero-3-phosphoethanolamine-*N*-[carboxy(polyethylene glycol)-2000] (DSPE-PEG(2000)-COOH) providing a functional carboxylic group and 1,2-distearoyl-*sn*-glycero-3-phosphoethanolamine-*N*-[amino(polyethylene glycol)-2000] (DSPE-PEG(2000)-NH_2), providing a functional amine, were also employed in the vesicle formulation. Here the polyethylene glycol chain (2000 Da) intercalated between the phospholipid headgroup and the respective functional group serves to enhance the colloidal stability of the resulting vesicle, as well as the protocells once formed.[24] Moreover, it is well-established that the presence of PEG chains on the particle surface improves the circulation time of the nanocarriers within the bloodstream.[25] These polymeric chains hamper the adsorption of the immune proteins

Scheme 1. Synthetic Pathway for the Production of Protocells
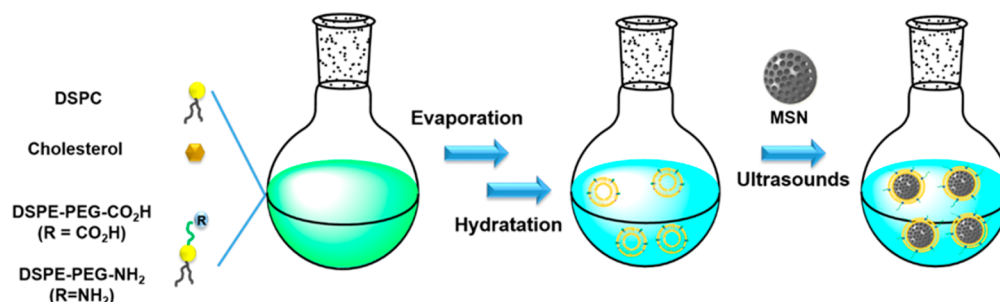
Scheme 2. Synthesis of Col$_{nc}$ (Upper Scheme) And Attachment Pathway of Col$_{nc}$ and Anti-EGFR-Biotin on PC Surface (Lower Scheme)
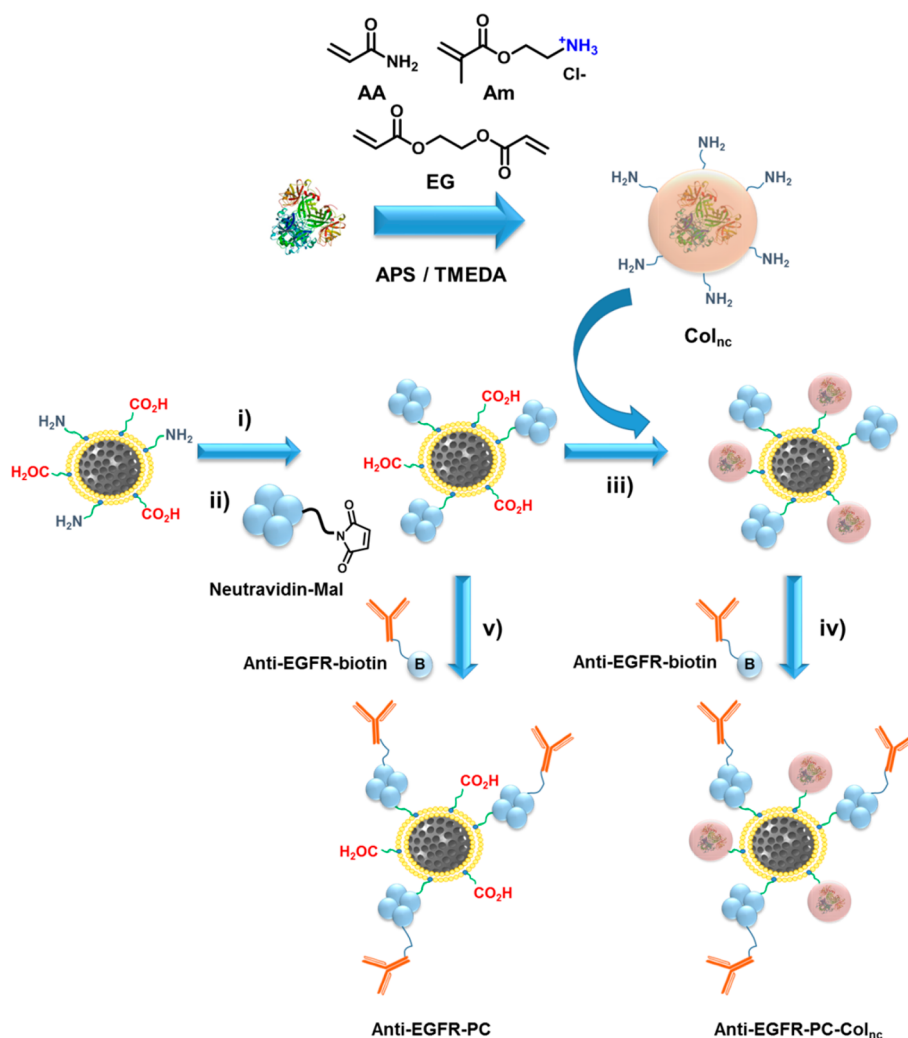
(opsonins) responsible for labeling foreign bodies for macrophage capture. Liposomes were synthesized following the thin-film hydration or Bangham method.[26] This method is based on the dissolution of various phospholipids in one organic phase followed by solvent evaporation, obtaining a lipid film. After that, the film is hydrated in a salt-rich aqueous medium under strong sonication, which results in the liposome formation. Two batches of vesicles were synthesized maintaining a fixed molar ratio of cholesterol to DSPE-PEG(2000)-NH$_2$ (20:2) and varying the molar ratio of DSPC and DSPE-PEG(2000)-COOH (65:13) and (48:30), respectively. The percentage of introduced

amino groups was kept constant at 2% because this percentage is sufficient for the antibody attachment as previously reported.[18] Thus, the two batches present different concentrations of carboxylic groups to determine the effect of the concentration of collagenase nanocapsules on penetration. Both vesicle batches were extruded to yield a monodisperse size distribution centered at 100 nm according to DLS measurements (DLS of DSPE-PEG(2000)-COOH (65:13) shows in Figure S2 as an example).

Two batches of protocells were prepared by incubating an aqueous suspension of MSN with vesicles of the respective formulation under strong sonication for 20 s in phosphate

buffered saline (PBS). Excess vesicles not fused to the silica surface were removed via centrifugation. Both protocell batches (PC−COOH13 and PC−COOH30, respectively) showed monodisperse sizes centered around 175 nm according to the DLS measurements (Figure S3). The presence of the lipid bilayer on the MSN surface was confirmed by TEM using phosphotungstic acid (PTA) as a staining agent (Figure 1b).[26] The thickness of the supported lipid bilayer was measured to be ∼4.7 nm on both batches ($n = 20$), which is in agreement with the values reported in the literature for 'protocell' systems.[18]

2.2. Synthesis of Collagenase Nanocapsules (Col$_{nc}$). As was mentioned in the introduction, tumor penetration is one of the most important challenges facing the field of nanomedicine. The diffusion of nanometric objects in a fluid is understood by the Stokes−Einstein equation ($D = KT/6\pi\eta r$), which indicates that the diffusion rate (D) is inversely proportional to the particle radius (r) and also to the viscosity of the media (η). Therefore, the diffusion of nanometric objects is clearly reduced by increasing particle size and the viscosity of the media. Many solid tumors exhibit overproduction of collagen, which accumulates within the extracellular matrix (ECM) and greatly impedes particle diffusion through the inner tumoral core. The intratumoral injection of proteolytic enzymes able to destroy these collagen accumulations partially alleviates this problem, but due to the labile nature of these enzymes, it is necessary to administer several dosages of them to achieve significant results. Our research group has reported the use of polymeric nanocapsules which contain enzymes encapsulated within an organic shell to preserve their catalytic function in the presence of aggressive agents such as temperature or other proteolytic enzymes.[27,28] Recently, collagenase has been encapsulated within pH-sensitive polymeric nanocapsules, which were designed to rapidly release the housed enzyme when the pH drops to the mild acidic conditions usually present in many tumoral tissues but retains the enzyme trapped within the polymeric matrix up to 24 h under normal physiological conditions.[16] Following the same methodology, collagenase polymeric nanocapsules were formed by a radical polymerization method which employs acrylamide (AA), as the main structural monomer, 2-aminoethyl methacrylate (Am) as the monomer that provides amino groups required for the further attachment on the protocell surface, and ethylenglycol dimethacrylate (EG) as pH-degradable cross-linker (Scheme 2).[29] In this process, monomer/protein molar ratios of 2419:1 and AA:Am:EG ratio (7:6:2) were employed.

The resulting nanocapsules were characterized by DLS measurements and TEM showing an average diameter of about 50 nm and a round-shaped morphology (Figure 1c). The employed polymer composition was selected to exhibit degradation by progressive hydrolysis over 24 h, which is accelerated in the mild-acidic conditions present in the tumor environment. The nanocapsule degradation at physiological pH was monitored by following decrease in hydrodynamic diameter over time. We observed that the collagenase nanocapsules initially of ∼50 nm in hydrodynamic diameter were progressively degraded until they reached a size of ∼7 nm, indicating the enzymes complete release after 24 h (Figure S4). The encapsulated collagenase retained its catalytic activity as was previously reported.[16]

2.3. Protocell Functionalization: Anchoring of Anti-EGFR and Collagenase Nanocapsules. To confer selectivity against tumoral cells, the nanoparticle surface was decorated with targeting moieties capable of being specifically recognized by cell membrane receptors overexpressed on the surface of cancerous cells. An EGFR antibody (anti-EGFR) was selected as a targeting ligand due to the common overexpression of EGFR in many human cancers, in particular lung cancer.[30,31] For this reason, A549 lung tumor cells were selected in this work as a cellular tumoral model. The anchoring of anti-EGFR and collagenase nanocapsules was carried out following a multistep synthetic process (Scheme 2).

The first step (i) was the conversion of the amino groups present on the protocell surface into thiol groups by the reaction with 2-iminothiolane hydrochloride (Traut's reagent). Then, these thiol groups were employed to anchor the maleimide-neutravidin moieties (ii). Thus, the protocells were ready for the antibody introduction employing biotinylated-Anti-EGFR (iv or v). Because of the sensitive nature of antibodies, collagenase nanocapsules were anchored (iii) prior to the introduction of antibody to preserve the recognition capacity of this macromolecule. As was mentioned above, two protocell batches displaying different percentages of carboxylic groups were synthesized (PC−COOH13 and PC−COOH30) to find the optimal composition which resulted in a higher collagenase nanocapsule attachment. Thus, collagenase nanocapsules were anchored on both types of protocells, using well-known carbodiimide chemistry (iii). The presence of collagenase nanocapsules was confirmed by measuring the enzymatic activity of the PC−COOH13-Col$_{nc}$ and PC−COOH30-Col$_{nc}$ respectively, using EnChekGelatinase/Collagenase Assay Kit. Both samples exhibited similar enzymatic activity and therefore, an increase in the amount of carboxylic groups on the PC surface did not improve the Col$_{nc}$ attachment (Figure S5). Additionally, the colloidal stability of PC−COOH13-Col$_{nc}$ was significantly higher than PC−COOH30-Col$_{nc}$, showing that the particles remained well suspended in PBS for more than 15 days. For these reasons, PC−COOH13-Col$_{nc}$ was selected as the best system for the further attachment of Anti-EGFR, which was carried out through the formation of a biotin-neutravidin bridge (iv and v).

2.4. *In Vitro* Evaluation of Protocell Targeting Capacity in 2D Model. As described above, Anti-EGFR was anchored on the protocell surface for improving the particle uptake within the tumoral cells. The capacity of these systems to selectively bind to tumoral cells was tested by employing 2D cultures of A549 lung cancer cells because these cells overexpress EGFR on their surface. A549 cells were exposed for 24 h to a fixed concentration of protocells (80 μg/mL) with and without the antibody anchored on their surface. After this time, the cells were gently washed with PBS to remove all noninternalized particles. The percentage of cells that had engulfed fluorescent nanoparticles was determined by flow cytometry thanks to the presence of rhodamine B covalently labeled within the silica matrix of the protocells (Figure 2).

The results confirmed the importance of the functionalization with the antibody because only 2% of the tumoral cells engulfed the protocells that did not present the antibody on their surface, whereas this value rose to over 90% when the antibody was present. In the complete system (Col$_{nc}$-PC-Anti-EGFR), collagenase nanocapsules were anchored prior to the antibody functionalization. This anchoring process requires carboxylic acid activation by carbodiimide chemistry, which could alter the neutravidin pockets due to the presence of carboxylic and amine groups in this protein and therefore could compromise the antibody conjugation. To evaluate this possibility, the cells were exposed to Col$_{nc}$-PC-Anti-EGFR and compared to the PC-Anti-
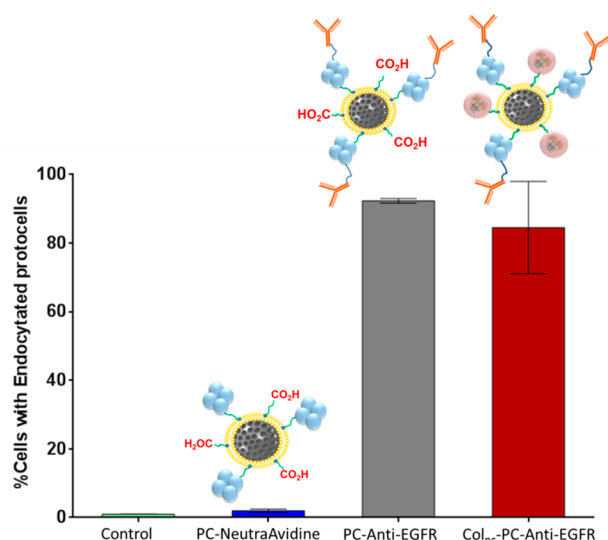
Figure 2. Cellular uptake of protocell with and without Anti-EGFR and Col$_{nc}$. Samples were performed in triplicate.

EGFR alone. Both the full construct, Col$_{nc}$-PC-Anti-EGFR, and PC-Anti-EGFR yielded similar uptake of 85% and >90%, respectively, confirming the suitability of this strategy for the synthesis of the complete nanodevice.

2.5. Evaluation of Penetration Capacity in 3D Tumoral Tissue Model. To evaluate the penetration capacity of these multifunctional protocells, a 3D tissue model that mimics the existing conditions in a solid tumoral mass was prepared. This model was based on the use of a 3D collagen gel containing embedded tumoral cells within its structure. This model presents similar consistency and rheological properties to human tumor tissue, and therefore, it can be employed as a simple substitute for a complex *in vivo* microenvironment.[32] Our model consisted of a monolayer of A549 cells on which a 3D collagen gel with embedded tumoral cells of 200 μm thickness was grown (Figure 3).

The gel mimics the ECM of the tumor and acts as barrier hindering the diffusion of protocells to the A549 monolayer.

Thus, to test the enhanced penetration of the system decorated with collagenase nanocapsules, a suspension of fluorescent protocells (80 μg/mL) bearing the antibody and prepared with or without collagenase nanocapsules, was carefully placed on the top of the gel. After 24 h of incubation, the gels were gently washed with PBS to remove the protocells which were unable to penetrate within/into the collagen matrix. The capacity to reach the bottom cell monolayer was assessed in each case by fluorescence confocal microscopy. The cell nuclei were stained with DAPI (blue) and, with the aim to assess that protocells were truly engulfed within the cell cytoplasm thanks to the presence of the targeting moiety, actin filaments were stained with green phalloidin. The confocal images show that only protocells functionalized with nanocapsules were able to reach the bottom layer, as can be observed by the existence of perinuclear red dots which correspond to the rhodamine B labeled MSN cores of the protocells. This result confirms the capacity of Col$_{nc}$-PC-Anti-EGFR to overcome the collagen barrier and reach deep layers of the tissue model. In addition, these protocells were found within the tumoral cell cytosol, which confirms the enhanced internalization of these nanocapsule-bearing protocells inside malignant cells. On the contrary, PC-Anti-EGFR were not able to overcome the collagen barrier and they were likely removed in the washing step, as can be observed by the absence of red dots (labeled nanocapsule-free protocells) in the cell layer.

2.6. Evaluation of Cytotoxic Capacity of Drug-Loaded Protocells in 3D Tumoral Tissue Model. Having established the ability of Col$_{nc}$-PC-Anti-EGFR to reach deep areas within a 3D tumoral model and once there, to be selectively internalized by tumoral cells, the ability of the system to transport and deliver cytotoxic drugs capable of inducing cell death was studied. Topotecan (TOP) is a potent antitumoral therapeutic but it suffers significant instability in the bloodstream losing its activity in a few hours.[33] For this reason, repeated dosages are required to maintain its concentration in the blood, which leads to severe side effects. It has been reported that the encapsulation of TOP within a nanocarrier improves its therapeutic efficacy.[34] For these reasons, topotecan was selected as drug model for this system. Col$_{nc}$-PC-Anti-EGFR were loaded prior to the
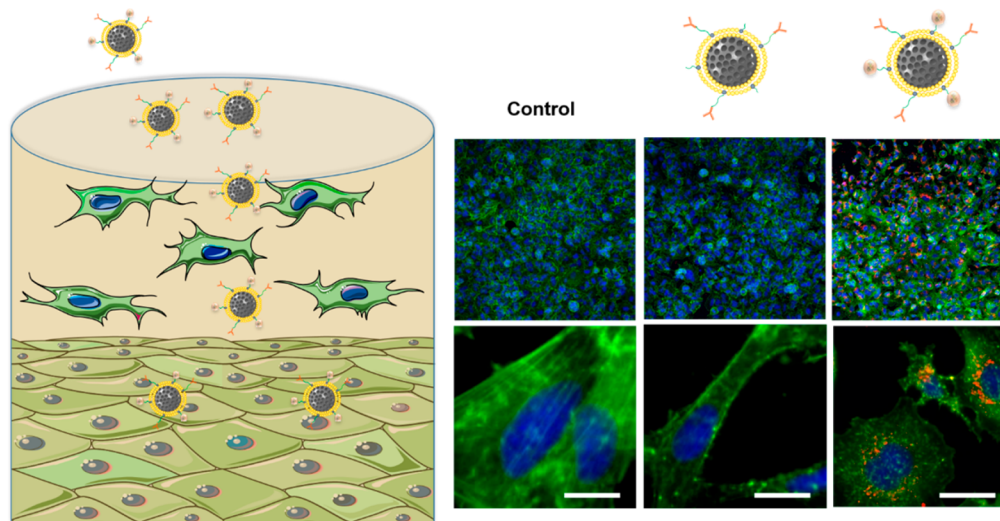

Figure 3. Evaluation of penetration and internalization capacity of PC-Anti-EGFR and Col$_{nc}$-PC-Anti-EGFR nanodevices, employing 3D tumoral tissue models. Cell nuclei are stained in blue, actin filaments were stained in green, and protocells were labeled in red (white bars correspond to 25 μm). Confocal fluorescent micrographs of each separate channel can be found in Supporting Information (Figure S6).
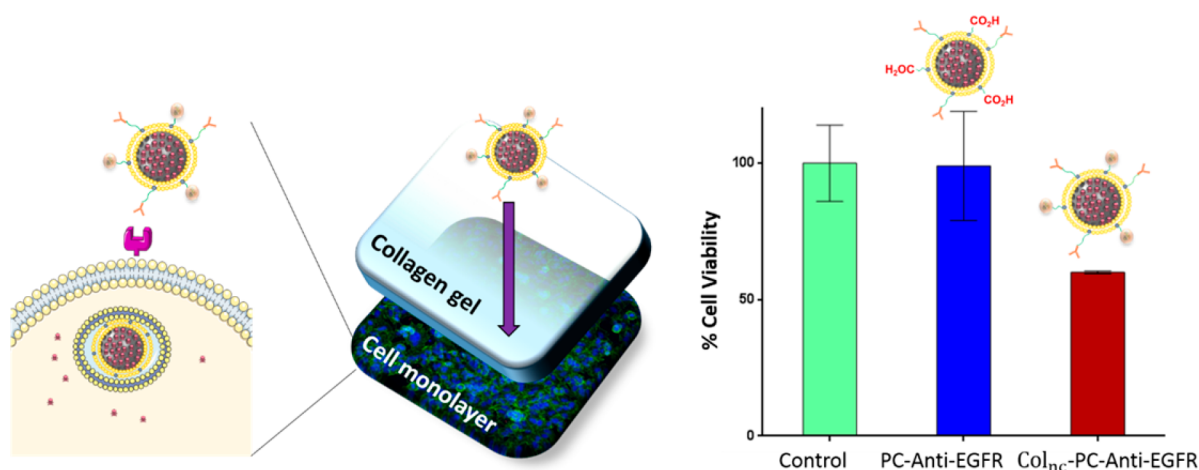
Figure 4. Cytotoxic capacity of Protocells in 3D tumoral tissue model after 24 h of incubation ($n = 3$, $p < 0.05$).

formation of the protocell by incubating the silica core for 24 h in an aqueous solution of topotecan (3 mg mL^{-1}). The loading capacity of the protocells was determined by differences in fluorescence between the topotecan solution, before and after the loading, yielding 0.6% (w:w) of cargo. A suspension of topotecan-loaded Col$_{nc}$-PC-Anti-EGFR was deposited on the surface of the 3D tumoral tissue model. PC-Anti-EGFR loaded with the same amount of topotecan was employed as a control to evaluate the cytotoxic capacity of protocells, which did not possess penetration capacity. After 24 and 48 h of incubation time, cell viability was evaluated by the Alamar blue viability assay. At 24 h, the results showed that topotecan-loaded Col$_{nc}$-PC-Anti-EGFR induced around 40% of cell mortality, whereas the system which did not contain the collagenase nanocapsules had negligible cytotoxicity (Figure 4). After 48 h, the cytotoxicity observed in the case of topotecan(TOP)-loaded Colnc-PC-Anti-EGFR reached up to 60% and PC-Anti-EGFR induced around 20% of cell destruction. The cytotoxicity provoked by this last nanodevice was probably caused by the small amount of TOP that leaks from protocells when they are exposed to physiological conditions over a relatively long timespan (Figure S7).[18] These results confirmed that the higher penetration capacity of collagenase nanocapsules results in significant improvements in the therapeutic efficacy of the cytotoxic compounds transported by these multifunctional protocells.

3. CONCLUSIONS

Herein, a multifunctional tumor-penetrating nanocarrier capable of selective delivery of antitumoral drugs to deep tumoral layers has been developed. This system is composed of mesoporous silica nanocarriers encapsulated within a supported lipid bilayer (aka protocell). The SLB of the protocell construct was modified with collagenase containing nanocapsules that serve to digest the highly dense tumoral extracellular matrix and enable protocell penetration. These collagenase nanocapsules were designed to protect the enzymatic activity of the collagenase until the target tissue is reached and then, to have pH-triggered (accelerated) release of collagenase within the tumoral area. Additionally, the "plug and play" feature of protocell surface allowed anchoring of EGFR antibodies, whose receptors are commonly overexpressed in human lung cancer cells, allowing a preferential internalization within tumoral cells. Thus, the system achieves highly efficient penetration within

dense matrix, selective internalization by tumoral cells and successful and controlled delivery of cytotoxic anticancer drugs. The importance of this system was highlighted by employing a 3D tumoral tissue model that mimics the extracellular matrix present in diseased tissues. Therefore, this system has demonstrated the capability to overcome one of the major problems of current nanomedicine, which is the limited penetration of nanosystems. The application of this strategy would pave the way for the design of smarter nanoconstructs able to achieve more homogeneous drug distribution within solid tumors, which is an important advance toward their clinical applications.

4. MATERIALS AND METHODS

4.1. Materials. Rhodamine B isothiocyanate (RBITC) (Sigma-Aldrich); Ethanol (Dismadel); (3-aminopropyl)triethoxysilane (APTES) (ABCR); Hexadecyltrimethylammonium bromide (CTAB) (Sigma-Aldrich); ammonium hydroxide (NH4OH, 28−30%) (Fluka); Tetraethyl orthosilicate (TEOS) (Aldrich); Ammonium nitrate (Sigma-Aldrich); 1,3-distearoyl-sn-glycero-3-phosphocholine (DSPC) (Avanti Lipids); 1,2-distearoyl-sn-glycero-3-phosphoethanolamine-N-[amino(polyethylene glycol)-2000] (ammonium salt) (DSPE-PEG(2000)-NH2) (Avanti Lipids); 1,2-distearoyl-sn-glycero-3-phosphoethanolamine-N-[carboxy(polyethylene glycol)-2000] (ammonium salt) (DSPE- PEG(2000)-COOH) (Avanti Lipids); Cholesterol (Avanti Lipids); Traut's reagent (Aldrich); Maleimide activated netrAvidin (thermo Scientific); biotinlyated EGFR antibody (Abcam); Collagenase Type I (Life Technologies); Acrylamide (Fluka); 2-Aminoethyl methacrylate hydrochloride (Sigma-Aldrich); Ethylene glycol dimethacrylate (Sigma-Aldrich); Ammonium persulfate (Sigma-Aldrich); N,N,N′,N′-Tetramethylethylenediamine (Sigma-Aldrich); AmiconUltra-2 mL Centrifugal Filters Ultracel-10K (Millipore); N-(3- Dimethylaminopropyl)-N′-ethylcarbodiimide hydrochloride (Sigma-Aldrich); N-Sulfo-Hydroxysuccidimide, (Sigma-Aldrich); EnChekGelatinase/Collagenase Assay Kit (Life Technologies); 10X PBS Buffer pH = 7.4 (Ambion); Dulbecco's modified Eagle's medium (Sigma-Aldrich); Rat tail collagen (type I) First Link (UK) Ltd.; Bovine serum albumin (BSA) (Sigma); Paraformaldehyde (Sigma-Aldrich); Atto488 phalloidine (Sigma-Aldrich); Triton X-100 (Aldrich); DAPI (Sigma); Topotecan (Sigma-Aldrich); Alamar blue (Invitrogen).

4.2. Instrumental Section. The hydrodynamic size of mesoporous nanoparticles and protein capsules was measured by means of a Zetasizer Nano ZS (Malvern Instruments) equipped with a 633 nm "red" laser. Transmission electron microscopy (TEM) was carried out with a JEOL TEM 3000 instruments operated at 300 kV, equipped with a CCD camera. Sample preparation was performed by dispersing MSN or protocells in pure ethanol or in distilled water, respectively, and

subsequent deposition onto holey carbon coated copper grids. A solution of 1% of phosphotungstic acid (PTA) pH 7.0 was employed as staining agent to visualize the protein capsules alone and attached on the mesoporous surface. Fluorescence was measured with Synergy 4, power supply for Biotek Laboratory Instrument 100−240VAC, 50/60 Hz, 250W. Confocal microscope Olympus FV1200 (Electron Microscopy Centre, UCM).

4.3. Synthesis of Mesoporous Silica Nanoparticles (MSN). To prepare dye-labeled mesoporous silica nanoparticles, 1.5 mg of Rhodamine B isothiocyanate (RBITC) was dissolved in 1 mL of ethanol and 1.5 μL of (3-aminopropyl)triethoxysilane (APTES) and the solution RBITC-APTES was keep at room temperature under magnetic stirring for 2 h. 0.290 g of hexadecyltrimethylammonium bromide (CTAB) was dissolved 150 g in ammonium hydroxide 0.32 M and the solution was incubated at 50 °C under magnetic stirring for 1 h in a 200 mL beaker sealed with parafilm. Then 3 mL of 0.88 M tetraethyl orthosilicate (TEOS) in ethanol and RBITC-APTES were added to the surfactant solution after adjusting the stirring speed to 650 rpm. The mixture was incubated at 50 °C under magnetic stirring for 1 h without parafilm, then the solution was aged at 50 °C overnight under static conditions. The next day, the particles were subjected to a hydrothermal treatment at 70 °C for 20 h before being collected by centrifugation and washed three times with water and ethanol. The surfactant was removed by placing the particles in 500 mL of a solution of 95% ethanol, 5% water, and 10 g of NH_4NO_3 mL^{-1} at 80 °C during 3 h with reflux and under stirring. The nanoparticles were washed with ethanol and were finally stored in pure ethanol.

4.4. Liposome Preparation. The lipids and cholesterol were solubilized in choloroform and were stored at −20 °C. To prepare liposomes, the corresponding lipids were mixed at mol % ratios: DSPC/Chol/DSPE-PEG(2000)-NH$_2$/DSPE- PEG(2000)-COOH = 65/20/2/13 and 48/20/2/30. The lipids were dried under vacuum to remove the organic solvent and obtain lipids film and were rehydrated in 1X PBS and bath sonicated for 1 h to obtain liposome solution. To obtain a monodispersed liposome solution, the liposomes were extruded using 0.05 μm polycarbonate filter membrane at least 21 times. Then monodispersed liposomes were obtained.

4.5. Synthesis of Protocells (PC−CO$_2$H13 and PC−CO$_2$H30). The silica nanoparticles were transferred to water at (2.5 mg/mL) from the ethanolic suspension by centrifugation (15 000 rpm, 10 min) and resuspension in water. To each batch of MSN, a suspension of liposomes 8×10^{-6} mol in 1.2 mL of PBS with 13% or 30% of carboxylic groups was added. The mixtures were sonicated for 20 s, and the excess of liposomes was removed by centrifugation (15 000 rpm, 10 min). The pelleted protocells were redispersed in PBS (1X) by sonication; this process was repeated two times. Finally, the protocells were stored in 1 mL of PBS (2.5 mg/mL).

4.6. Synthesis of Collagenase Capsule (Col$_{nc}$). First, the reaction buffer NaHCO$_3$ (0.01 M, pH 8.5) was deoxygenated by freeze-vacuum-N$_2$ cycles. Then collagenase (3.1×10^{-5} mmol) was dissolved in the freshly deoxygenated buffer. In a separated vial, 0.035 mmol of acrylamide (AA), 0.030 mmol of 2-aminoethyl metacrylate hydrochloride (Am), and 0.010 mmol of ethylene glycol dimetacrylate (EG) were dissolved in 1 mL of deoxygenated buffer and the monomer solution was added to the protein solution. This mixture was stirred at 300 rpm for 10 min under nitrogen atmosphere at room temperature. Then 0.013 mmol of ammonium persulfate and 0.02 mmol of N,N,N',N'-tetramethyl ethylenediamine (TMDA) dissolved in 1 mL of the deoxygenated buffer was added. The solution was stirred at 300 rpm for 90 min at room temperature under inert atmosphere. Next, the encapsulated enzyme was purified by centrifugal separation with 10 kDa cutoff filters (AMICON Ultra-2 mL 10 kDa) and washed three times with NaHCO$_3$ buffer (0.01 M pH 8.5). The capsules of collagenase were preserved at 4 °C.

4.7. Protocells Functionalization with Anti-EGFR and Col$_{nc}$.
4.7.1. Conversion of NH$_2$ Groups into SH Groups. A 125 μL sample of 250 mM Traut's reagent in PBS was added to the protocells. The reaction was kept for 2 h under stirring at room temperature. After this time, the excess of Traut's reagent was removed via centrifugation (15 000 rpm, 10 min) and the pellet of protocells was resuspended in PBS. This step was repeated twice. Finally, the thiol-functionalized protocells were stored in 1 mL of PBS (2.5 mg mL^{-1}).

4.7.2. Attachment of NeutrAvidin. A 0.5 mL sample of (1 mg mL^{-1} in water) maleimide-functionalized NeutrAvidin protein was added to 1 mL (2.5 mg mL^{-1}) of thiol-functionalized protocells. The reaction was incubated under stirring at room temperature during 12 h. After this time, the excess of maleimide-functionalized NeutrAvidin was removed via centrifugation (15 000 rpm, 10 min) and the protocells pellet was resuspended in 1X PBS. This step was carried out twice. PC-NeutrAvidin were stored in 1 mL of 1X PBS (2.5 mg mL^{-1}) at 4 °C.

4.7.3. Synthesis of Col$_{nc}$-PC. The carboxylic groups of PC-NeutrAvidin (0.6 mL of 2.5 mg.mL^{-1} in NaHCO$_3$ buffer (0.01 M, pH 8.5)) were activated by adding 2.5 mg of N-(3-(dimethylamino)-propyl)-N'-ethylcarbodiimide hydrochloride (EDC) and 2.5 mg of N-hydroxysulfosuccidimide (NHS). To maintain the basic conditions, 2.5 mg of NaHCO$_3$ was added to the mixture. The sample was placed in an orbital stirrer at 400 rpm during 10 min. After this time, 4 mg of collagenase nanocapsules was added, and the mixture was stirred during 4 h. Col$_{nc}$-PC-NeutrAvidin were collected by centrifugation and washed three times with PBS. Col$_{nc}$-PC-NeutrAvidin were stored at 4 °C.

4.7.4. Synthesis of Col$_{nc}$-PC-Anti-EGFR. Twenty-five micrograms of biotinlyated Anti-EGFR was mixed with 250 μg of PC-NeutrAvidin or Col$_{nc}$-PC-NeutrAvidin Protocells, respectively, during 1 h at room temperature. After this time, protocells were isolated by centrifugation (15 000 rpm, 10 min) and they were redispersed in 250 μL of PBS (1X) yielding PC-Anti-EGFR or Col$_{nc}$-PC-Anti-EGFR, respectively.

4.8. Cell Culture and Targeting Studies in 2D. Protocell selective uptake of each system were evaluated in 2D cell culture model and flow cytometry. For this study, 20 000 A549 cells cm^{-2} were seeded into each well of a 24-well plate. The cells were incubated with 80 μg of the corresponding protocell (PC-NetrAvidin or PC-Anti-EGFR) left untreated (control) during 24 h at 37 °C at 5% CO$_2$ atmospheric concentration. Then the cells were washed two times with PBS (1X) to remove the noninternalized protocells and then the cells were treated with trypsin and the percentages of cells that have internalized fluorescence protocells were measured by flow cytometry using a BD FACSCaliber flow cytometer. Samples were performed in triplicate, and 10 000 cells were assessed per sample. To calculate the percent of cells positive for the protocells, a gate was set to contain 1% of control cells. This gate was then applied to all other samples to determine the percent of cells positive for protocells.

4.9. Enzymatic Activity Measurements. The enzymatic activity of all samples were evaluated following the protocol EnChekGelatinase/Collagenase Assay Kit.

4.10. Preparation of 3D Tumoral Tissue Models Based on A549-Seeded Collagen Gels. For this study, 20 000 A549 cells cm^{-2} were seeded in 24-well plate. A 0.5 mL sample of complete media was added to each well, and the cells were cultured at 37 °C at 5% CO$_2$ atmospheric concentration for 24 h. Then the collagen gel with A549 cells embedded into the collagen matrix was directly prepared in contact with the cell monolayer. For this purpose, 5.32 mL of rat tail collagen type I (3 mg mL^{-1}) and 15.48 mL of complete medium (Dulbecco's modified Eagle's medium complemented with 10% of FBS) were mixed at 0 °C. Then 100 μL of sodium hydroxide was added to obtain a mixture with neutral pH. Five milliliters of FBS, 5 mL of complete medium, and 5 mL of a solution of cells of concentration A549 1.7×10^6 cell mL^{-1} were added to the neutral collagen solution, keeping the temperature at 0 °C. The mixture was pipetted into 24-well plates (0.25 mL per well) and incubated at 37 °C at 5% CO$_2$ atmospheric concentration for 1 day to promote gel formation. Then 250 μL of complete medium was added in each well, and the gel was incubated at 37 °C at 5% CO$_2$ atmospheric concentration overnight. These gels were used for the further experiments 2 days after gel formation.

4.11. Study of Penetration and Cell Internalization in A549-Seeded Collagen Gels. To study the penetration of nanocarriers in 3D tumoral tissue models, 80 μL of suspended PC-Anti-EGFR and Col$_{nc}$-PC-Anti-EGFR (1 mg mL^{-1}) was respectively added on top of each gel. These samples were incubated at 37 °C at 5% CO$_2$

atmospheric concentration during 24 h. Then the supernatant was removed and the gel was washed twice with PBS. Then 0.5 mL of a solution 4% paraformaldehyde and 1% sucrose in PBS was added to each well and incubated for 20 min. After this time, the wells were washed two times with PBS 1X and 0.5 mL of a solution of 0.5% triton X-100 in PBS was added and the wells were incubated during 5 min at room temperature to permeate the cell membrane. Then the wells were washed with PBS and incubated for 20 min at 37 °C with a solution of BSA 1% in PBS. After this step, BSA was removed and 0.5 mL of a solution of 30 μL of ATTO488 phalloidine solution (1 mg mL^{-1} in methanol) in 1 mL of BSA1%, was added. The wells were incubated for 40 min and washed two times with PBS (1X). Then 0.5 mL of one solution of DAPI in PBS (0.1 μg/mL) was added, and the wells were incubated during 15 min at room temperature. Finally, the excess of DAPI was removed washing two times with PBS (1X). The samples were ready for observation by fluorescent confocal microscopy.

4.12. Topotecan Loading. One milliliter of ethanolic suspension of MSN (2.5 mg mL^{-1}) was washed two times with water and finally was resupended in 0.5 mL of an aqueous solution of topotecan (5 mg mL^{-1}) during 12 h. The excess of topotecan was removed by centrifugation (15 000 rpm, 10 min) and two washing steps in H$_2$O. The amount of topotecan housed in MSN was determined by the difference in fluorescence in the initial cargo solution and the resulting supernatant. These topotecan-loaded MSN were employed for the drug-loaded protocell following the method described above.

4.13. Cell Viability Studies. The cytotoxic capacity of these multifunctional protocells was evaluated using the same 3D tumoral tissue model mentioned above. Briefly, 80 μL of each drug-loaded protocell (1 mg mL^{-1}) was added on the top of 3D gels with cells A549 embedded. These gels were incubated at 37 °C at 5% CO$_2$ atmospheric concentration during 24 h. The supernatant was removed, and the gel was washed two times with PBS (1X). Then 0.5 mL of Alamar Blue solution (10%) in cell culture medium was added to each well, and the gels were incubated at 37 °C at 5% CO$_2$ atmospheric concentration during 1 h. Finally, the fluorescence of supernatant was measured using λ_{ex} = 570 nm and λ_{em} = 585 nm using a microplate reader.

ASSOCIATED CONTENT

Supporting Information

The Supporting Information is available free of charge on the ACS Publications website at DOI: 10.1021/acs.chemmater.7b03128.

Hydrodynamic diameter of mesoporous silica nanoparticles, liposomes, and protocells obtained by DLS, study of collagenase nanocapsules hydrolysis under physiological conditions, enzymatic activity of different types of protocells, and each separate channel of confocal fluorescent micrographs (PDF)

AUTHOR INFORMATION

Corresponding Authors
*E-mail: abaezaga@ucm.es.
*E-mail: cjbrink@sandia.gov.
*E-mail: vallet@ucm.es.

ORCID
Alejandro Baeza: 0000-0002-9042-8865
C. Jeffrey Brinker: 0000-0002-7145-9324

Author Contributions
The manuscript was written through contributions of all authors. All authors have given approval to the final version of the manuscript.

Notes
The authors declare no competing financial interest.

REFERENCES

(1) Siegel, R. L.; Miller, K. D.; Jemal, A. Cancer Statistics. *Ca-Cancer J. Clin.* **2016**, *66*, 7−30.

(2) Hanahan, D.; Weinberg, R. A. Hallmarks of Cancer: The Next Generation. *Cell* **2011**, *144*, 646−674.

(3) Matsumura, Y.; Maeda, H. A New Concept for Macromolecular Therapeutics in Cancer-Chemotherapy - Mechanism of Tumoritropic Accumulation of Proteins and the Antitumor Agent Smancs. *Cancer Res.* **1986**, *46*, 6387−6392.

(4) Liu, D.; Auguste, D. T. Cancer Targeted Therapeutics: From Molecules to Drug Delivery Vehicles. *J. Controlled Release* **2015**, *219*, 632−643.

(5) Maeda, H. Toward a Full Understanding of the EPR Effect in Primary and Metastatic Tumors as Well as Issues Related to Its Heterogeneity. *Adv. Drug Delivery Rev.* **2015**, *91*, 3−6.

(6) Ediriwickrema, A.; Saltzman, W. M. Nanotherapy for Cancer: Targeting and Multifunctionality in the Future of Cancer Therapies. *ACS Biomater. Sci. Eng.* **2015**, *1*, 64−78.

(7) Mura, S.; Nicolas, J.; Couvreur, P. Stimuli-Responsive Nanocarriers for Drug Delivery. *Nat. Mater.* **2013**, *12*, 991−1003.

(8) Karakoti, A. S.; Das, S.; Thevuthasan, S.; Seal, S. PEGylated Inorganic Nanoparticles. *Angew. Chem., Int. Ed.* **2011**, *50*, 1980−1994.

(9) Xu, X.; Ho, W.; Zhang, X.; Bertrand, N.; Farokhzad, O. Cancer Nanomedicine: From Targeted Delivery to Combination Therapy. *Trends Mol. Med.* **2015**, *21*, 223−232.

(10) Sun, T.-M.; Wang, Y.-C.; Wang, F.; Du, J.-Z.; Mao, C.-Q.; Sun, C.-Y.; Tang, R.-Z.; Liu, Y.; Zhu, J.; Zhu, Y.-H.; et al. Cancer Stem Cell Therapy Using Doxorubicin Conjugated to Gold Nanoparticles via Hydrazone Bonds. *Biomaterials* **2014**, *35*, 836−845.

(11) Wilhelm, S.; Tavares, A. J.; Dai, Q.; Ohta, S.; Audet, J.; Dvorak, H. F.; Chan, W. C. W. Analysis of Nanoparticle Delivery to Tumours. *Nat. Rev. Mater.* **2016**, *1*, 16014.

(12) Florence, A. T. Targeting" Nanoparticles: The Constraints of Physical Laws and Physical Barriers. *J. Controlled Release* **2012**, *164*, 115−124.

(13) Netti, P. a; Berk, D. a; Swartz, M. a; Grodzinsky, a J.; Jain, R. K. Role of Extracellular Matrix Assembly in Interstitial Transport in Solid Tumors. *Cancer Res.* **2000**, *60*, 2497−2503.

(14) McKee, T. D.; Grandi, P.; Mok, W.; Alexandrakis, G.; Insin, N.; Zimmer, J. P.; Bawendi, M. G.; Boucher, Y.; Breakefield, X. O.; Jain, R. K. Degradation of Fibrillar Collagen in a Human Melanoma Xenograft Improves the Efficacy of an Oncolytic Herpes Simplex Virus Vector. *Cancer Res.* **2006**, *66*, 2509−2513.

(15) Parodi, A.; Haddix, S. G.; Taghipour, N.; Scaria, S.; Taraballi, F.; Cevenini, A.; Yazdi, I. K.; Corbo, C.; Palomba, R.; Khaled, S. Z.; et al. Bromelain Surface Modification Increases the Diffusion of Silica Nanoparticles in the Tumor Extracellular Matrix. *ACS Nano* **2014**, *8*, 9874−9883.

(16) Villegas, M. R.; Baeza, A.; Vallet Regí, M. Hybrid Collagenase Nanocapsules for Enhanced Nanocarrier Penetration in Tumoral Tissues. *ACS Appl. Mater. Interfaces* **2015**, *7*, 24075−24081.

(17) Nguyen, K. T.; Zhao, Y. Engineered Hybrid Nanoparticles for On-Demand Diagnostics and Therapeutics. *Acc. Chem. Res.* **2015**, *48*, 3016−3025.

(18) Durfee, P. N.; Lin, Y.-S.; Dunphy, D. R.; Muñiz, A. J.; Butler, K. S.; Humphrey, K. R.; Lokke, A. J.; Agola, J. O.; Chou, S. S.; Chen, I.-M.; et al. Mesoporous Silica Nanoparticle-Supported Lipid Bilayers (Protocells) for Active Targeting and Delivery to Individual Leukemia Cells. *ACS Nano* **2016**, *10*, 8325−8345.

(19) Butler, K. S.; Durfee, P. N.; Theron, C.; Ashley, C. E.; Carnes, E. C.; Brinker, C. J. Protocells: Modular Mesoporous Silica Nanoparticle-Supported Lipid Bilayers for Drug Delivery. *Small* **2016**, *12*, 2173−2185.

(20) Ashley, C. E.; Carnes, E. C.; Epler, K. E.; Padilla, D. P.; Phillips, G. K.; Castillo, R. E.; Wilkinson, D. C.; Wilkinson, B. S.; Burgard, C. A.; Kalinich, R. M.; et al. Delivery of Small Interfering RNA by Peptide-Targeted Mesoporous Silica Nanoparticle-Supported Lipid Bilayers. *ACS Nano* **2012**, *6*, 2174−2188.

(21) Vallet-Regi, M.; Rámila, A.; del Real, R. P.; Pérez-Pariente, J. A New Property of MCM-41: Drug Delivery System. *Chem. Mater.* **2001**, *13*, 308−311.

(22) Vallet-Regi, M.; Balas, F.; Arcos, D. Mesoporous Materials for Drug Delivery. *Angew. Chem., Int. Ed.* **2007**, *46*, 7548−7558.

(23) Nussbaumer, S.; Bonnabry, P.; Veuthey, J.-L.; Fleury-Souverain, S. Analysis of Anticancer Drugs: A Review. *Talanta* **2011**, *85*, 2265−2289.

(24) Lin, Y.-S.; Haynes, C. L. Impacts of Mesoporous Silica Nanoparticle Size, Pore Ordering, and Pore Integrity on Hemolytic Activity. *J. Am. Chem. Soc.* **2010**, *132*, 4834−4842.

(25) He, Q.; Zhang, J.; Shi, J.; Zhu, Z.; Zhang, L.; Bu, W.; Guo, L.; Chen, Y. The Effect of PEGylation of Mesoporous Silica Nanoparticles on Nonspecific Binding of Serum Proteins and Cellular Responses. *Biomaterials* **2010**, *31*, 1085−1092.

(26) Bozzuto, G.; Molinari, A. Liposomes as Nanomedical Devices. *Int. J. Nanomed.* **2015**, *10*, 975.

(27) Bello, V.; Mattei, G.; Mazzoldi, P.; Vivenza, N.; Gasco, P.; Idee, J. M.; Robic, C.; Borsella, E. Transmission Electron Microscopy of Lipid Vesicles for Drug Delivery: Comparison between Positive and Negative Staining. *Microsc. Microanal.* **2010**, *16*, 456−461.

(28) Baeza, A.; Guisasola, E.; Torres-Pardo, A.; González-Calbet, J. M.; Melen, G. J.; Ramirez, M.; Vallet-Regí, M. Hybrid Enzyme-Polymeric Capsules/Mesoporous Silica Nanodevice for In Situ Cytotoxic Agent Generation. *Adv. Funct. Mater.* **2014**, *24*, 4625−4633.

(29) Simmchen, J.; Baeza, A.; Ruiz-Molina, D.; Vallet-Regí, M. Improving Catalase-Based Propelled Motor Endurance by Enzyme Encapsulation. *Nanoscale* **2014**, *6*, 8907−8913.

(30) Berger, M. S.; Gullick, W. J.; Greenfield, C.; Evans, S.; Addis, B. J.; Waterfield, M. D. Epidermal Growth Factor Receptors in Lung Tumours. *J. Pathol.* **1987**, *152*, 297−307.

(31) Noh, M. S.; Lee, S.; Kang, H.; Yang, J. K.; Lee, H.; Hwang, D.; Lee, J. W.; Jeong, S.; Jang, Y.; Jun, B.-H.; Jeong, D. H.; Kim, S. K.; Lee, Y.-S.; Cho, M.-H. Target-specific near-IR induced drug release and photothermal therapy with accumulated Au/Ag hollow nanoshells on pulmonary cancer cell membranes. *Biomaterials* **2015**, *45*, 81−92.

(32) Child, H. W.; Del Pino, P. a.; De La Fuente, J. M.; Hursthouse, A. S.; Stirling, D.; Mullen, M.; McPhee, G. M.; Nixon, C.; Jayawarna, V.; Berry, C. C. Working Together: The Combined Application of a Magnetic Field and Penetratin for the Delivery of Magnetic Nanoparticles to Cells in 3D. *ACS Nano* **2011**, *5*, 7910−7919.

(33) Herben, V. M.; ten Bokkel Huinink, W. W.; Beijnen, J. H. Clinical Pharmacokinetics of Topotecan. *Clin. Pharmacokinet.* **1996**, *31*, 85−102.

(34) Drummond, D. C.; Noble, C. O.; Guo, Z.; Hayes, M. E.; Connolly-Ingram, C.; Gabriel, B. S.; Hann, B.; Liu, B.; Park, J. W.; Hong, K. Development of a Highly Stable and Targetable Nano-liposomal Formulation of Topotecan. *J. Controlled Release* **2010**, *141*, 13−21.